Available online at www.sciencedirect.com
SCIENCE DIRECT®
Comput. Methods Appl. Mech. Engrg. 194 (2005) 2947–2968
Computer methods in applied mechanics and engineering
www.elsevier.com/locate/cma

An analysis of some mixed-enhanced finite element for plane linear elasticity

F. Auricchio [a,b], L. Beirão da Veiga [c], C. Lovadina [b,c,*], A. Reali [a,d]

[a] *Dipartimento di Meccanica Strutturale, Università di Pavia, Via Ferrata 1, Pavia I-27100, Italy*
[b] *IMATI-CNR, Via Ferrata 1, Pavia I-27100, Italy*
[c] *Dipartimento di Matematica, Università di Pavia, Via Ferrata 1, Pavia I-27100, Italy*
[d] *European School for Advanced Studies in Reduction of Seismic Risk (ROSE School), Università di Pavia, Via Ferrata 1, Pavia I-27100, Italy*

Received 2 October 2003; received in revised form 15 July 2004; accepted 28 July 2004

Abstract

The paper investigates Mixed-Enhanced Strain finite elements developed within the context of the *u*/*p* formulation for nearly incompressible linear elasticity problems. A rigorous convergence and stability analysis is detailed, providing also L^2-error estimates for the displacement field. Extensive numerical tests are developed, showing in particular the accordance of the computational results with the theoretical predictions.

Keywords: Nearly-incompressible elasticity; Displacement/pressure formulation; Finite element methods; Enhanced strain technique; Nonconforming methods; Error analysis

1. Introduction

In this paper we study some *Enhanced Strain* finite element methods for nearly incompressible linear elasticity problems. Introduced by Simo and Rifai (cf. [20]), the Enhanced Strain Technique, essentially consists in augmenting the space of discrete strains with local functions, which may not derive from admissible displacements. A suitable choice of these additional modes can improve the numerical performance of

* Corresponding author. Address: Dipartimento di Matematica, Università di Pavia, Via Ferrata 1, Pavia I-27100, Italy. Tel.: +39 0382 505685; fax: +39 0382 505602.
E-mail address: lovadina@dimat.unipv.it (C. Lovadina).

0045-7825/$ - see front matter
doi:10.1016/j.cma.2004.07.028

low-order elements and, more importantly, it can greatly alleviate the well-known *volumetric locking* phenomenon in the nearly-incompressible regime.

Several theoretical contributions about the Enhanced Strain technique are nowadays available in the literature. The first one is probably the work by Reddy and Simo [16], where a priori error estimates have been developed starting from the Hu–Washizu variational principle. In Ref. [3], Braess provided an extensive study concerning the effect of the strain enhancement on the resulting stiffness matrix. This analysis has been improved in [4], where λ-uniform error estimates for the displacement field have been established. However, uniform error estimates for the volumetric part of the stress field could not be obtained, since the corresponding *mixed* method does not satisfy the inf–sup condition (cf [5]). In [13] Pantuso and Bathe applied the Enhanced Strain philosophy in the framework of the displacement/pressure formulation for elasticity problems (cf. e.g. [2,5,9]). They proposed a four-noded quadrilateral element which indeed satisfies the inf–sup condition, thus leading to an optimally convergent method, as theoretically proved in [10].

It is interesting to notice that most of the schemes taking advantage of the Enhanced Strain technique have been designed in connection with *quadrilateral* elements. This because, when *displacement-based* (low-order) triangular elements are considered, the additional strain degrees of freedom do not provide any improvement, as highlighted in [16]. On the other hand (cf. [11]), the mixed *displacement/pressure* formulation opens the possibility to select effective *triangular* enhanced strain modes. We also wish to remark that triangular enhanced strains have already been used by Piltner and Taylor in [15] for a low-order element with rotational degrees of freedom.

The main aim of this paper is to investigate on the numerical performance of the triangular mixed-enhanced methods briefly presented in [11]. We also develop a general theoretical analysis which can be considered as an extension of the results presented in [10]; in particular, we provide optimal uniform error bounds both for the natural norms (H^1 for the displacements and L^2 for the pressure), and for the L^2-norm of the displacements.

The structure of the work is as follows. In Section 2 we recall the mixed displacement/pressure formulation for the deformation problem of a linearly elastic body, together with its discretization by means of the Enhanced Strain technique. In Section 3 we develop our stability and convergence analysis, while in Section 4 we show that two examples of triangular elements, briefly presented in [11], actually fall into the framework of our theory. Finally, in Section 5 we develop extensive and significant numerical tests, showing the computational performance of our elements. In particular, we show the accordance of the numerical results with the theoretical predictions by means of two incompressible elasticity problems for which the analytical solution is known.

Throughout the paper we will use standard notation, especially for Sobolev norms and seminorms (cf. e.g. [5,7]).

2. The linear elasticity problem

We consider the plane linear elasticity problem in the framework of the infinitesimal theory (cf. [2]) for a homogeneous isotropic material. Within the several possible formulations of the problem we adopt the *mixed* displacement/pressure formulation (cf. [2,5,9], for instance). If the elastic body occupy a regular region Ω in $\mathbf{R}^2$ with boundary $\partial\Omega$, we are therefore led to solve the following boundary-value problem:

Find $(\underline{u},p)$ such that

$$\begin{cases} -\underline{\mathrm{div}}\,(2\mu\underline{\underline{\varepsilon}}(\underline{u}) + p\underline{\underline{\delta}}) = \underline{f} & \text{in } \Omega \\ \mathrm{div}\,\underline{u} - \lambda^{-1}p = 0 & \text{in } \Omega \\ \underline{u} = 0 & \text{on } \partial\Omega. \end{cases} \tag{1}$$

where $\underline{u} = (u_1,u_2): \Omega \to \mathbf{R}^2$ is the displacement field, $p: \Omega \to \mathbf{R}$ is the pressure field and $\underline{f} = (f_1,f_2): \Omega \to \mathbf{R}^2$ is the loading term. Moreover, $\underline{\underline{\varepsilon}}(\cdot)$ is the usual symmetric gradient operator acting on vector fields, while $\underline{\underline{\delta}}$ is the second-order identity tensor. Finally, μ and λ are the Lamé coefficients, for which we suppose that $0 < \mu_0 \leqslant \mu \leqslant \mu_1 < +\infty$ and $0 < \lambda_0 \leqslant \lambda \leqslant +\infty$. We notice that $\lambda = +\infty$ (and therefore $\lambda^{-1} = 0$ in (1)) refers to the case of an incompressible material.

Remark 1. For simplicity, we consider only homogeneous boundary conditions for the displacement field along the whole $\partial\Omega$, but most of the subsequent results can be extended to other more realistic situations.

A standard variational formulation of problem (1) consists in finding $(\underline{u}, p) \in V \times P = (H_0^1(\Omega))^2 \times L^2(\Omega)/\mathbf{R}$ which solves the system

$$\begin{cases} 2\mu \displaystyle\int_\Omega \underline{\underline{\varepsilon}}(\underline{u}) : \underline{\underline{\varepsilon}}(\underline{v}) + \int_\Omega p \operatorname{div} \underline{v} = \int_\Omega \underline{f} \cdot \underline{v} & \forall \underline{v} \in V \\ \displaystyle\int_\Omega q \operatorname{div} \underline{u} - \lambda^{-1} \int_\Omega pq = 0 & \forall q \in P. \end{cases} \tag{2}$$

Remark 2. In the case of homogeneous Dirichlet boundary conditions for $\underline{u}$ on the whole $\partial\Omega$, we work with the space $P = L^2(\Omega)/\mathbf{R} = \{q \in L^2(\Omega) : \int_\Omega q = 0\}$ because, from (1) we get

$$\int_\Omega p = \lambda \int_\Omega \operatorname{div} \underline{u} = \lambda \int_{\partial\Omega} \underline{u} \cdot \underline{n} = 0.$$

Therefore, for every choice of $\underline{f}$ and λ, the pressure solution p is always in P.

It is well-known that problem (2) is well-posed and it fits into the theory extensively studied in [5], for instance. We recall that the nearly-incompressible case, we mainly focus on, corresponds to λ "very large" compared to μ. We also notice that in the incompressible *limit* $\lambda \to \infty$, formulation (2) does not degenerate, leading to the following Stokes-like problem:

Find $(\underline{u}_0, p_0) \in V \times P$ such that

$$\begin{cases} 2\mu \displaystyle\int_\Omega \underline{\underline{\varepsilon}}(\underline{u}_0) : \underline{\underline{\varepsilon}}(\underline{v}) + \int_\Omega p_0 \operatorname{div} \underline{v} = \int_\Omega \underline{f} \cdot \underline{v} & \forall \underline{v} \in V \\ \displaystyle\int_\Omega q \operatorname{div} \underline{u}_0 = 0 & \forall q \in P. \end{cases} \tag{3}$$

2.1. Enhanced strain discretization

It is now well-established (cf. [2,5]) that the finite element analysis of problem (2) requires some care in the case of nearly-incompressible materials. This fact is highlighted by the *limit* situation (3), where the divergence-free constraint imposes a suitable choice of the discretization spaces, in order to overcome the so-called *volume locking phenomenon*. Several methods have been proposed, analyzed and proved to be efficient in actual computations (cf. [2,5,9] and the references therein). Among them, there are the ones based on the *Enhanced Strain Technique*, whose basic idea is briefly recalled below.

As usual, given a regular (triangular or quadrilateral) mesh $\mathcal{T}_h$ of Ω, h being the mesh-size, we choose a finite element space $V_h \subset V$ for the approximation of the displacements, and a finite element space $P_h \subset P$ for the pressure field. A *conforming* mixed method is thus given by the discrete problem

Find $(\underline{u}_h,p_h) \in V_h \times P_h$ such that

$$\begin{cases} 2\mu \int_\Omega \underline{\underline{\varepsilon}}(\underline{u}_h) : \underline{\underline{\varepsilon}}(\underline{v}_h) + \int_\Omega p_h \operatorname{div} \underline{v}_h = \int_\Omega \underline{f} \cdot \underline{v}_h & \forall \underline{v}_h \in V_h, \\ \int_\Omega q_h \operatorname{div} \underline{u}_h - \lambda^{-1} \int_\Omega p_h q_h = 0 & \forall q_h \in P_h. \end{cases} \tag{4}$$

An *Enhanced Strain Method* in this mixed context can be seen as a *nonconforming and inconsistent* scheme (cf. [10]), for which the strains arising from the displacements are "enriched" by means of some additional modes. Therefore, we are led to introduce a further finite element space E_h of symmetric tensors, and we solve the problem

Find $(\underline{u}_h, \tilde{\underline{\underline{\varepsilon}}}_h, p_h) \in V_h \times E_h \times P_h$ such that

$$\begin{cases} 2\mu \int_\Omega (\underline{\underline{\varepsilon}}(\underline{u}_h) + \tilde{\underline{\underline{\varepsilon}}}_h) : (\underline{\underline{\varepsilon}}(\underline{v}_h) + \tilde{\underline{\underline{\tau}}}_h) + \int_\Omega p_h (\operatorname{div} \underline{v}_h + \operatorname{tr} \tilde{\underline{\underline{\tau}}}_h) = \int_\Omega \underline{f} \cdot \underline{v}_h, \\ \int_\Omega q_h (\operatorname{div} \underline{u}_h + \operatorname{tr} \tilde{\underline{\underline{\varepsilon}}}_h) - \lambda^{-1} \int_\Omega p_h q_h = 0. \end{cases} \tag{5}$$

for every $(\underline{v}_h, \tilde{\underline{\underline{\tau}}}_h) \in V_h \times E_h$ and for every $q_h \in P_h$. Above and in the sequel, we denote with "tr" the trace operator acting on tensors. The space E_h of strain enhancement typically consists of functions for which *no continuity* is required across the mesh elements. As a consequence, a static condensation procedure can be performed at the element level, so that the introduction of these additional degrees of freedom does not severely increase the computational costs. More importantly, the enhanced strains can improve the stability of the method at hand, leading to a *robust scheme* with respect to the choice of the material parameter λ. Therefore, the resulting element can be successfully applied to both compressible and incompressible case.

The inconsistency of the scheme is clearly seen by inserting the *analytical* solution $(\underline{u},p)$ of problem (2) into (5). As the *analytical* strain enhancement is obviously $\underline{\underline{0}}$, we have that $(\underline{u},\underline{\underline{0}},p)$ fails to satisfy the first equation of (5), because

$$2\mu \int_\Omega \underline{\underline{\varepsilon}}(\underline{u}) : \tilde{\underline{\underline{\tau}}}_h + \int_\Omega p \operatorname{tr} \tilde{\underline{\underline{\tau}}}_h = 0 \quad \forall \tilde{\underline{\underline{\tau}}}_h \in E_h \tag{6}$$

does not generally hold true. This drawback can be overcome by suitably choosing the space E_h, as detailed in the next Section.

3. Error analysis

In this Section we present an analysis for the methods based on the Enhanced Strain Technique. Since the stability estimate of Proposition 3 and the error bound of Theorem 4 have been already established in [10] for the incompressible limit case, we only sketch the proofs, for the sake of completeness. However, in Section 3.1 we develop L^2-norm displacement error estimates, which, to our best knowledge, have not explicitly appeared in the existing literature for the Enhanced Strain Technique.

Before proceeding, we introduce in $V_h \times E_h$ the following norm:

$$\|(\underline{v}_h, \tilde{\underline{\underline{\tau}}}_h)\| = (|\underline{\underline{\varepsilon}}(\underline{v}_h)|_0^2 + |\tilde{\underline{\underline{\tau}}}_h|_0^2)^{1/2}. \tag{7}$$

Moreover, we endow $V_h \times E_h \times P_h$ with the norm

$$|||(\underline{v}_h, \tilde{\underline{\underline{\tau}}}_h, q_h)||| := (\|(\underline{v}_h, \tilde{\underline{\underline{\tau}}}_h)\|^2 + |q_h|_0^2)^{1/2}. \tag{8}$$

We finally introduce the notation

$$b_h(\underline{v}_h, \underline{\tilde{\tau}}_h; q_h) := \int_\Omega q_h(\operatorname{div} \underline{v}_h + \operatorname{tr} \underline{\tilde{\tau}}_h), \tag{9}$$

for every $(\underline{v}_h, \underline{\tilde{\tau}}_h) \in V_h \times E_h$ and $q_h \in P_h$.

The basic assumptions we make on the choice of the discretization spaces V_h, E_h and P_h are the following (cf. [10] and also [16]).

- *The discrete inf–sup condition*: there exists a positive constant β, independent of h, such that

$$\inf_{q_h \in P_h} \sup_{(\underline{v}_h, \underline{\tilde{\tau}}_h) \in V_h \times E_h} \frac{b_h(\underline{v}_h, \underline{\tilde{\tau}}_h; q_h)}{|||(\underline{v}_h, \underline{\tilde{\tau}}_h)||| \, |q_h|_0} \geqslant \beta. \tag{10}$$

- *The minimum angle condition*: there exists a constant $\theta < 1$, independent of h, such that

$$\sup_{(\underline{v}_h, \underline{\tilde{\tau}}_h) \in V_h \times E_h} \frac{\int_\Omega \underline{\underline{\varepsilon}}(\underline{v}_h) : \underline{\underline{\tilde{\tau}}}_h}{|\underline{\underline{\varepsilon}}(\underline{v}_h)|_0 |\underline{\underline{\tilde{\tau}}}_h|_0} \leqslant \theta. \tag{11}$$

  This condition implies, in particular, that $\underline{\underline{\varepsilon}}(V_h) \cap E_h = (0)$. Moreover, the spaces $\underline{\underline{\varepsilon}}(V_h)$ and E_h "stays far from being parallel" uniformly in h. We remark that condition (11) has been recognized to be crucial for the analysis of enhanced strain methods also in [3].
- *The approximation property*: there exists an integer $k \geqslant 1$ such that for $\underline{v} \in H^{k+1}(\Omega)^2$ and $q \in H^k(\Omega)$, it holds

$$\inf_{\underline{v}_h \in V_h} \|\underline{v} - \underline{v}_h\|_1 + \inf_{q_h \in P_h} |q - q_h|_0 \leqslant Ch^k(|\underline{v}|_{k+1} + |q|_k). \tag{12}$$

  Obviously, this condition is fulfilled by the standard (triangular or quadrilateral) finite element space of order k (see [7]).
- *The consistency condition*: in each element the enhanced strain modes should be L^2-orthogonal to the polynomials of order up to $k-1$, i.e. for every $K \in \mathscr{T}_h$

$$\int_K \underline{\underline{\tilde{\tau}}}_h : \underline{\underline{p}}_{k-1} = 0 \quad \forall \underline{\underline{\tilde{\tau}}}_h \in E_h, \forall \underline{\underline{p}}_{k-1} \in \mathscr{P}_{k-1}(K)^4_s. \tag{13}$$

  This condition allows to control the consistency error arising from the introduction of the space E_h (cf. (6)).

For the sake of notational simplicity, in the sequel we will denote with $(\cdot,\cdot)$ the usual inner product in L^2. Moreover, we introduce the bilinear form $\mathscr{A}_h(\cdot,\cdot,\cdot;\cdot,\cdot,\cdot)$ on $V_h \times E_h \times P_h$ by setting

$$\mathscr{A}_h(\underline{v}_h, \underline{\tilde{\tau}}_h, q_h; \underline{w}_h, \underline{\tilde{\sigma}}_h, r_h) := 2\mu(\underline{\underline{\varepsilon}}(\underline{v}_h) + \underline{\underline{\tilde{\tau}}}_h, \underline{\underline{\varepsilon}}(\underline{w}_h) + \underline{\underline{\tilde{\sigma}}}_h) + b_h(\underline{w}_h, \underline{\tilde{\sigma}}_h; q_h) - b_h(\underline{v}_h, \underline{\tilde{\tau}}_h; r_h) + \lambda^{-1}(q_h, r_h), \tag{14}$$

for any $(\underline{v}_h, \underline{\tilde{\tau}}_h, q_h)$ and $(\underline{w}_h, \underline{\tilde{\sigma}}_h, r_h)$ in $V_h \times E_h \times P_h$. The discrete scheme can thus be written as

Find $(\underline{u}_h, \underline{\tilde{\varepsilon}}_h, p_h) \in V_h \times E_h \times P_h$ such that

$$\mathscr{A}_h(\underline{u}_h, \underline{\tilde{\varepsilon}}_h, p_h; \underline{v}_h, \underline{\tilde{\tau}}_h, q_h) = (\underline{f}, \underline{v}_h) \quad \forall (\underline{v}_h, \underline{\tilde{\tau}}_h, q_h) \in V_h \times E_h \times P_h. \tag{15}$$

We have the following stability result.

Proposition 3. *Provided that (10) and (11) hold, for each* $(\underline{v}_h, \underline{\tilde{\tau}}_h, q_h) \in V_h \times E_h \times P_h$ *there exists* $(\underline{w}_h, \underline{\tilde{\sigma}}_h, r_h) \in V_h \times E_h \times P_h$ *such that*

$$|||(\underline{w}_h, \underline{\tilde{\sigma}}_h, r_h)||| \leqslant c_1 |||(\underline{v}_h, \underline{\tilde{\tau}}_h, q_h)|||, \tag{16}$$

$$\mathscr{A}_h(\underline{v}_h, \underline{\tilde{\tau}}_h, q_h; \underline{w}_h, \underline{\tilde{\sigma}}_h, r_h) \geqslant c_2 |||(\underline{v}_h, \underline{\tilde{\tau}}_h, q_h)|||^2, \tag{17}$$

with c_1 and c_2 constants independent of h and λ.

Proof. Fix $(\underline{v}_h, \underline{\tilde{\tau}}_h, q_h) \in V_h \times E_h \times P_h$. We first notice that the inf–sup condition (10) implies the existence of $(\underline{z}_h, \underline{\tilde{\rho}}_h) \in V_h \times E_h$ such that

$$[\![(\underline{z}_h, \underline{\tilde{\rho}}_h)]\!] \leqslant \beta^{-1} |q_h|_0, \quad b_h(\underline{z}_h, \underline{\tilde{\rho}}_h; q_h) = |q_h|_0^2. \tag{18}$$

We will choose

$$(\underline{w}_h, \underline{\tilde{\sigma}}_h, r_h) = (\underline{v}_h, \underline{\tilde{\tau}}_h, q_h) + \delta(\underline{z}_h, \underline{\tilde{\rho}}_h, 0)$$

where δ is a positive parameter still at our disposal. We have

$$\mathscr{A}_h(\underline{v}_h, \underline{\tilde{\tau}}_h, q_h; \underline{w}_h, \underline{\tilde{\sigma}}_h, r_h) = \mathscr{A}_h(\underline{v}_h, \underline{\tilde{\tau}}_h, q_h; \underline{v}_h, \underline{\tilde{\tau}}_h, q_h) + \delta \mathscr{A}_h(\underline{v}_h, \underline{\tilde{\tau}}_h, q_h; \underline{z}_h, \underline{\tilde{\rho}}_h, 0) \tag{19}$$

Using (11) and (14) it follows

$$\mathscr{A}_h(\underline{v}_h, \underline{\tilde{\tau}}_h, q_h; \underline{w}_h, \underline{\tilde{\sigma}}_h, r_h) \geqslant C_1 [\![(\underline{v}_h, \underline{\tilde{\tau}}_h)]\!]^2 + \delta \mathscr{A}_h(\underline{v}_h, \underline{\tilde{\tau}}_h, q_h; \underline{z}_h, \underline{\tilde{\rho}}_h, 0). \tag{20}$$

Furthermore, using (18) and Young's inequality, we obtain for every $\delta_1 > 0$

$$\begin{aligned} \mathscr{A}_h(\underline{v}_h, \underline{\tilde{\tau}}_h, q_h; \underline{z}_h, \underline{\tilde{\rho}}_h, 0) &= 2\mu(\underline{\varepsilon}(\underline{v}_h) + \underline{\tilde{\tau}}_h, \underline{\varepsilon}(\underline{z}_h) + \underline{\tilde{\rho}}_h) + |q_h|_0^2 \\ &\geqslant -\frac{C_2 \delta_1}{2} [\![(\underline{v}_h, \underline{\tilde{\tau}}_h)]\!]^2 + \left(1 - \frac{C_2 \beta^{-2}}{2\delta_1}\right) |q_h|_0^2. \end{aligned} \tag{21}$$

Taking $\delta_1 = C_2 \beta^{-2}$ we have

$$\mathscr{A}_h(\underline{v}_h, \underline{\tilde{\tau}}_h, q_h; \underline{z}_h, \underline{\tilde{\rho}}_h, 0) \geqslant -\frac{C_2^2 \beta^{-2}}{2} [\![(\underline{v}_h, \underline{\tilde{\tau}}_h)]\!]^2 + \frac{1}{2} |q_h|_0^2. \tag{22}$$

From (20) and (22) we obtain

$$\mathscr{A}_h(\underline{v}_h, \underline{\tilde{\tau}}_h, q_h; \underline{w}_h, \underline{\tilde{\sigma}}_h, r_h) \geqslant \left(C_1 - \delta \frac{C_2^2 \beta^{-2}}{2}\right) [\![(\underline{v}_h, \underline{\tilde{\tau}}_h)]\!]^2 + \frac{\delta}{2} |q_h|_0^2. \tag{23}$$

Therefore, choosing $\delta > 0$ sufficiently small we get (17). The continuity condition (16) is straightforward. □

We remark that in the stability result of Proposition 3, implying in particular existence and uniqueness of problem (5), the consistency condition (13) does not appear. It however comes into play in the following error estimate.

Theorem 4. *Assume that conditions (10)–(13) hold true. Let $(\underline{u},p) \in V \times P$ be the solution of problem (2) and suppose that*

$$\|\underline{u}\|_{k+1} + \|p\|_k \leqslant C, \tag{24}$$

with C constant independent of λ. Let $(\underline{u}_h, \underline{\tilde{\varepsilon}}_h, p_h) \in V_h \times E_h \times P_h$ be the solution of the discrete problem (5). Then it holds

$$\|\underline{u} - \underline{u}_h\|_1 + |\underline{\tilde{\varepsilon}}_h|_0 + |p - p_h|_0 \leqslant C h^k, \tag{25}$$

with C constant independent of lambda.

Proof. Take $(\underline{v}_h, q_h) \in V_h \times P_h$ and consider $(\underline{u}_h - \underline{v}_h, \underline{\tilde{\varepsilon}}_h, p_h - q_h)$. From Proposition 3, there exists $(\underline{w}_h, \underline{\tilde{\sigma}}_h, r_h) \in V_h \times E_h \times P_h$ such that

$$|||(\underline{w}_h, \underline{\tilde{\sigma}}_h, r_h)||| \leqslant c_1 |||(\underline{u}_h - \underline{v}_h, \underline{\tilde{\varepsilon}}_h, p_h - q_h)|||, \tag{26}$$

$$\mathscr{A}_h(\underline{u}_h - \underline{v}_h, \underline{\tilde{\varepsilon}}_h, p_h - q_h; \underline{w}_h, \underline{\tilde{\sigma}}_h, r_h) \geqslant c_2 |||(\underline{u}_h - \underline{v}_h, \underline{\tilde{\varepsilon}}_h, p_h - q_h)|||^2. \tag{27}$$

Moreover, it is easily seen that

$$\begin{aligned}\mathscr{A}_h(\underline{u}_h - \underline{v}_h, \underline{\tilde{\varepsilon}}_h, p_h - q_h; \underline{w}_h, \underline{\tilde{\sigma}}_h, r_h) = {} & 2\mu(\underline{\varepsilon}(\underline{u} - \underline{v}_h), \underline{\varepsilon}(\underline{w}_h) + \underline{\tilde{\sigma}}_h) + (p - q_h, \operatorname{div} \underline{w}_h + \operatorname{tr} \underline{\tilde{\sigma}}_h) \\ & - (r_h, \operatorname{div}(\underline{u} - \underline{v}_h)) + \lambda^{-1}(p - q_h, r_h) - 2\mu(\underline{\varepsilon}(\underline{u}), \underline{\tilde{\sigma}}_h) - (p, \operatorname{tr} \underline{\tilde{\sigma}}_h).\end{aligned} \tag{28}$$

We only treat the last two terms, since the others can be handled in a standard way. Let us denote with $\Pi\underline{\varepsilon}(\underline{u})$ (resp. Πp) the L^2-projection of $\underline{\varepsilon}(\underline{u})$ (resp. p) over the piecewise polynomial functions of order up to $k-1$. Using (13), (24) and usual approximation results, we have

$$(\underline{\varepsilon}(\underline{u}), \underline{\tilde{\sigma}}_h) = (\underline{\varepsilon}(\underline{u}) - \Pi\underline{\varepsilon}(\underline{u}), \underline{\tilde{\sigma}}_h) \leqslant Ch^k |\underline{u}|_{k+1} |\underline{\tilde{\sigma}}_h|_0 \leqslant Ch^k |\underline{\tilde{\sigma}}_h|_0 \tag{29}$$

and

$$(p, \operatorname{tr} \underline{\tilde{\sigma}}_h) = (p - \Pi p, \operatorname{tr} \underline{\tilde{\sigma}}_h) \leqslant Ch^k |p|_k |\underline{\tilde{\sigma}}_h|_0 \leqslant Ch^k |\underline{\tilde{\sigma}}_h|_0. \tag{30}$$

From (26)–(28) we thus obtain

$$|||(\underline{u}_h - \underline{v}_h, \underline{\tilde{\varepsilon}}_h, p_h - q_h)||| \leqslant C_1 \Big(\inf_{\underline{v}_h \in V_h} \|\underline{u} - \underline{v}_h\|_1 + \inf_{q_h \in P_h} |p - q_h|_0 \Big) + C_2 h^k. \tag{31}$$

Error estimate (25) now follows from (7) to (8), Korn's inequality, assumption (12), (24) and the triangle inequality. □

Remark 5. We notice that the last two terms in (28) arise from the inconsistency of the Enhanced Strain Technique (cf. (6)). These extra terms are however under control by assumption (13), as highlighted by (29) and (30).

3.1. L^2-error estimates

We now prove an L^2-error estimate for the displacement field. We recall that Theorem 4 gives

$$\|\underline{u} - \underline{u}_h\|_1 + |\underline{\tilde{\varepsilon}}_h|_0 + |p - p_h|_0 \leqslant Ch^k. \tag{32}$$

In this situation we show that the displacement error in L^2-norm is $O(h^{k+1})$, provided the problem is regular. More precisely, we assume that for the solution of the problem:

Find $(\underline{\varphi}, s) \in V \times P$ such that

$$\begin{cases} 2\mu(\underline{\varepsilon}(\underline{v}), \underline{\varepsilon}(\underline{\varphi})) + (s, \operatorname{div} \underline{v}) = (\underline{g}, \underline{v}) & \forall \underline{v} \in V \\ (q, \operatorname{div} \underline{\varphi}) - \lambda^{-1}(q, s) = 0 & \forall q \in P, \end{cases} \tag{33}$$

the regularity result

$$\|\underline{\varphi}\|_2 + \|s\|_1 \leqslant C|\underline{g}|_0 \tag{34}$$

holds true for every $\underline{g} \in L^2(\Omega)^2$.

Remark 6. The regularity estimate (34) holds whenever Ω is a smooth domain, as proved in [21]. In the case of zero boundary conditions for the displacements on the whole boundary $\partial\Omega$, this result still holds when Ω is a convex polygon (cf. [6]).

Proposition 7. *Assume that conditions (10)–(13) are fulfilled. Moreover, assume (12) and the regularity estimate (34) for problem (33). Then we have the error bound*

$$|\underline{u} - \underline{u}_h|_0 \leqslant Ch^{k+1} \tag{35}$$

with C constant independent of λ.

Proof. Take $\underline{g} = \underline{u} - \underline{u}_h$ and $\underline{v} = \underline{u} - \underline{u}_h$ in the first equation of (33). We obtain

$$\|\underline{\varphi}\|_2 + \|s\|_1 \leqslant C|\underline{u} - \underline{u}_h|_0 \quad \text{(cf. (34))} \tag{36}$$

and

$$|\underline{u} - \underline{u}_h|_0^2 = 2\mu(\underline{\underline{\varepsilon}}(\underline{u} - \underline{u}_h), \underline{\underline{\varepsilon}}(\underline{\varphi})) + (s, \operatorname{div}(\underline{u} - \underline{u}_h)). \tag{37}$$

Let $\underline{\varphi}_I \in V_h$ (resp. $s_I \in P_h$) be an interpolant of $\underline{\varphi}$ (resp. s) satisfying (see [7])

$$\begin{cases} \|\underline{\varphi} - \underline{\varphi}_I\|_1 \leqslant Ch|\underline{\varphi}|_2, \\ |s - s_I|_0 \leqslant Ch|s|_1. \end{cases} \tag{38}$$

Taking into account that $(\underline{u},p)$ solve (2) and $(\underline{u}_h, \underline{\tilde{\varepsilon}}_h, p_h)$ solve (5), we get

$$-2\mu(\underline{\underline{\varepsilon}}(\underline{u} - \underline{u}_h), \underline{\underline{\varepsilon}}(\underline{\varphi}_I)) - (p - p_h, \operatorname{div}\underline{\varphi}_I) + 2\mu(\underline{\tilde{\varepsilon}}_h, \underline{\underline{\varepsilon}}(\underline{\varphi}_I)) = 0. \tag{39}$$

Similarly, we have

$$-(s_I, \operatorname{div}(\underline{u} - \underline{u}_h)) + \lambda^{-1}(p - p_h, s_I) + (s_I, \operatorname{tr}\underline{\tilde{\varepsilon}}_h) = 0. \tag{40}$$

From (37)–(40) we obtain

$$\begin{aligned} |\underline{u} - \underline{u}_h|_0^2 = {} & 2\mu(\underline{\underline{\varepsilon}}(\underline{u} - \underline{u}_h), \underline{\underline{\varepsilon}}(\underline{\varphi} - \underline{\varphi}_I)) + (s - s_I, \operatorname{div}(\underline{u} - \underline{u}_h)) - (p - p_h, \operatorname{div}\underline{\varphi}_I) \\ & + \lambda^{-1}(p - p_h, s_I) + 2\mu(\underline{\tilde{\varepsilon}}_h, \underline{\underline{\varepsilon}}(\underline{\varphi}_I)) + (s_I, \operatorname{tr}\underline{\tilde{\varepsilon}}_h). \end{aligned} \tag{41}$$

Moreover, since $\operatorname{div}\underline{\varphi} - \lambda^{-1}s = 0$ we have

$$\begin{aligned} |\underline{u} - \underline{u}_h|_0^2 = {} & 2\mu(\underline{\underline{\varepsilon}}(\underline{u} - \underline{u}_h), \underline{\underline{\varepsilon}}(\underline{\varphi} - \underline{\varphi}_I)) + (s - s_I, \operatorname{div}(\underline{u} - \underline{u}_h)) - (p - p_h, \operatorname{div}(\underline{\varphi}_I - \underline{\varphi})) \\ & + \lambda^{-1}(p - p_h, s_I - s) + 2\mu(\underline{\tilde{\varepsilon}}_h, \underline{\underline{\varepsilon}}(\underline{\varphi}_I)) + (s_I, \operatorname{tr}\underline{\tilde{\varepsilon}}_h) \\ = {} & T_1 + T_2 + T_3 + T_4 + T_5 + T_6. \end{aligned} \tag{42}$$

Estimates (32), (38), Cauchy–Schwarz inequality, and (36) lead to

$$T_1 \leqslant 2\mu|\underline{\underline{\varepsilon}}(\underline{u} - \underline{u}_h)|_0|\underline{\underline{\varepsilon}}(\underline{\varphi} - \underline{\varphi}_I)|_0 \leqslant Ch^{k+1}|\underline{\varphi}|_2 \leqslant Ch^{k+1}|\underline{u} - \underline{u}_h|_0. \tag{43}$$

The terms T_2–T_4 can be handled in the same way to obtain

$$T_i \leqslant Ch^{k+1}|\underline{u} - \underline{u}_h|_0 \quad i = 1, \ldots, 4. \tag{44}$$

To treat T_5 and T_6 we notice that, due to (13), we have

$$T_5 + T_6 = 2\mu(\underline{\tilde{\varepsilon}}_h, \underline{\underline{\varepsilon}}(\underline{\varphi}_I) - \underline{\underline{\varepsilon}}(\underline{\varphi})) + 2\mu\left(\underline{\tilde{\varepsilon}}_h, \underline{\underline{\varepsilon}}(\underline{\varphi}) - \overline{\underline{\underline{\varepsilon}}(\underline{\varphi})}\right) + (s_I - s, \operatorname{tr}\underline{\tilde{\varepsilon}}_h) + (s - \overline{s}, \operatorname{tr}\underline{\tilde{\varepsilon}}_h), \tag{45}$$

where $\overline{\underline{\underline{\varepsilon}}(\varphi)}$ (resp. $\overline{s}$) is the L^2-projection of $\underline{\underline{\varepsilon}}(\underline{\varphi})$ (resp. s) over the piecewise constant functions. Recalling that $|\underline{\tilde{\varepsilon}}_h|_0 \leqslant Ch_k$ (cf. (32)), Cauchy–Schwarz inequality, bounds (38) and (36) lead to

$$T_5 + T_6 \leqslant Ch^{k+1}|\underline{u} - \underline{u}_h|_0. \tag{46}$$

Estimate (35) is now a consequence of (42), (44) and (46). □

4. Examples of triangular elements

In this Section we introduce two sets of (first order) enhanced strains to be used in connection with *triangular* elements, already presented and briefly analyzed in [11]. We thus suppose to have a regular triangular mesh $\mathscr{T}_h$ of Ω. The schemes we are going to present are both based on the following choice of spaces:

- for the displacement discretization we take
$$V_h = \{v_h \in V : v_{h|T} \in \mathscr{P}_1(T) \quad \forall T \in \mathscr{T}_h\}, \tag{47}$$
where $\mathscr{P}1(T)$ is the space of linear functions defined on T;
- for the pressure interpolation, we set
$$P_h = \left\{q_h \in H^1(\Omega) : q_{h|T} \in \mathscr{P}_1(T) \quad \forall T \in \mathscr{T}_h\right\}. \tag{48}$$

We notice that, as for the Pantuso–Bathe element described in [13], the discrete pressure field is *continuous* across adjacent elements. Before introducing the two sets of enhanced strains, we first define a global Cartesian system of coordinates (x,y) in Ω. Furthermore, for each triangle $T \in \mathscr{T}_h$, let (x_T,y_T) be the coordinates of its barycenter, and define on T a *local* Cartesian system of coordinates by simply setting

$$\bar{x} = x - x_T, \quad \bar{y} = y - y_T. \tag{49}$$

We are now ready to present our strain enhancements.

- **First set**. We take
$$E_h^1 = \left\{\tilde{\underline{\underline{\tau}}}_h \in (L^2(\Omega))_s^4 : \tilde{\underline{\underline{\tau}}}_{h|T} \in E_4^1(T) \quad \forall T \in \mathscr{T}_h\right\}, \tag{50}$$
where $E_4^1(T)$ is the space of tensor-valued functions defined on T, spanned by the following shape functions (cf. (49))
$$\begin{bmatrix} \alpha_1\bar{x} + \alpha_2\bar{y}; & (\alpha_2 - \alpha_4)\bar{x} + (\alpha_3 - \alpha_1)\bar{y} \\ \text{symm.}; & \alpha_3\bar{x} + \alpha_4\bar{y} \end{bmatrix} \quad \text{with } \alpha_i \in \mathbf{R}. \tag{51}$$
We remark that the enhanced strain modes described in (51) have already been used in [15].
- **Second set**. We take
$$E_h^2 = \left\{\tilde{\underline{\underline{\tau}}}_h \in (L^2(\Omega))_s^4 : \tilde{\underline{\underline{\tau}}}_{h|T} \in E_4^2(T) \quad \forall T \in \mathscr{T}_h\right\}, \tag{52}$$
where $E_4^2(T)$ is the space of tensor-valued functions defined on T, spanned by the following shape functions (cf. (49))
$$\begin{bmatrix} \alpha_1\bar{x}; & \alpha_2\bar{x} + \alpha_3\bar{y} \\ \text{symm.}; & \alpha_4\bar{y} \end{bmatrix} \quad \text{with } \alpha_i \in \mathbf{R}. \tag{53}$$
We remark that this choice is not frame invariant. However, a strategy to make the results at least independent of the user's input data is detailed in [15].

We now prove that our discretization spaces fulfill the basic conditions (10)–(13). We consider only the first set of enhanced strains (51), since the other case can be treated using analogous techniques.

Proposition 8. *The choice* (47), (48), (50), (51) *satisfies conditions* (10)–(13) *with* $k = 1$.

Proof. First of all, notice that by construction conditions (12) and (13) are satisfied with $k = 1$. Moreover, take $\underline{v}_h \in V_h$ and $\underline{\underline{\tilde{\tau}}}_h \in E_h^1$. The symmetric gradient $\underline{\underline{\varepsilon}}(\underline{v}_h)$ is constant on each $T \in \mathscr{T}_h$, so that

$$\int_\Omega \underline{\underline{\varepsilon}}(\underline{v}_h) : \underline{\underline{\tilde{\tau}}}_h = 0. \tag{54}$$

It turns out that condition (11) holds, with $\theta = 0$. It remains to verify the inf–sup condition (10). To this end, we will use Fortin's criterion (cf. [5]). In our framework, we thus want to build a linear operator $\Pi_h : V \to V_h \times E_h^1$ such that

$$\lfloor \Pi_h \underline{v} \rfloor \leqslant C \|\underline{v}\|_1 \quad \forall \underline{v} \in V \tag{55}$$

and

$$b_h(\Pi_h \underline{v}; q_h) = \int_\Omega q_h \operatorname{div} \underline{v} \quad \forall \underline{v} \in V, \quad \forall q_h \in P_h. \tag{56}$$

We first define $\Pi_1 : V \to V_h$ as the standard Clément's operator (cf. [8]). Next, we search for a linear operator $\Pi_2 : V \to V_h \times E_h^1$ such that

$$b_h(\Pi_2 \underline{v}; q_h) = \int_\Omega q_h \operatorname{div} \underline{v} \quad \forall \underline{v} \in V, \quad \forall q_h \in P_h. \tag{57}$$

Given $\underline{v} \in V$, we will set $\Pi_2 \underline{v} = (0, \underline{\underline{\tilde{\sigma}}}_h) \in V_h \times E_h^1$, for a suitable $\underline{\underline{\tilde{\sigma}}}_h$ dependent on $\underline{v}$. Therefore, the operator Π_2 will be valued only on E_h^1 and condition (57) specializes as

$$\int_\Omega q_h \operatorname{tr} \underline{\underline{\tilde{\sigma}}}_h = \int_\Omega q_h \operatorname{div} \underline{v} \quad \forall \underline{v} \in V, \quad \forall q_h \in P_h. \tag{58}$$

Since the pressure interpolation is continuous, from (58) we see that we need to solve:

Given $\underline{v} \in V$, find $\underline{\underline{\tilde{\sigma}}}_h \in E_h^1$ such that

$$\int_\Omega q_h \operatorname{tr} \underline{\underline{\tilde{\sigma}}}_h = -\int_\Omega \underline{\nabla} q_h \cdot \underline{v} \quad \forall q_h \in P_h. \tag{59}$$

On each $T \in \mathscr{T}_h$, we locally define $\underline{\underline{\tilde{\sigma}}}_h$ by taking $\underline{\underline{\tilde{\sigma}}}_T$ as the *unique* solution in $E_4^1(T)$ (cf. (51)) of

$$\begin{cases} \underline{\underline{\tilde{\sigma}}}_T^D := \underline{\underline{\tilde{\sigma}}}_T - \dfrac{\operatorname{tr} \underline{\underline{\tilde{\sigma}}}_T}{2} \underline{\underline{\delta}} = 0 \\ \displaystyle\int_T q_1 \operatorname{tr} \underline{\underline{\tilde{\sigma}}}_T = -\int_T \underline{\nabla} q_1 \cdot \underline{v} \quad \forall q_1 \in \mathscr{P}_1(T)/\mathbf{R}. \end{cases} \tag{60}$$

Setting $\bar{q}_h$ as the L^2-projection of q_h over the piecewise constant functions, by property (13) and (60) we have

$$\begin{aligned} \int_\Omega q_h \operatorname{tr} \underline{\underline{\tilde{\sigma}}}_h &= \int_\Omega (q_h - \bar{q}_h) \operatorname{tr} \underline{\underline{\tilde{\sigma}}}_h = \sum_{T \in \mathscr{T}_h} \int_T (q_h - \bar{q}_h) \operatorname{tr} \underline{\underline{\tilde{\sigma}}}_T = -\sum_{T \in \mathscr{T}_h} \int_T \underline{\nabla} (q_h - \bar{q}_h) \cdot \underline{v} \\ &= -\sum_{T \in \mathscr{T}_h} \int_T \underline{\nabla} q_h \cdot \underline{v} = -\int_\Omega \underline{\nabla} q_h \cdot \underline{v} \quad \forall q_h \in P_h, \end{aligned} \tag{61}$$

i.e. $\underline{\underline{\tilde{\sigma}}}_h \in E_h^1$ is a solution of system (59). Hence, the operator $\Pi_2 : V \to V_h \times E_h^1$ defined by $\Pi_2 \underline{v} = (0, \underline{\underline{\tilde{\sigma}}}_h)$ satisfies (57).

Moreover, taking $q_1 = \operatorname{tr} \underline{\underline{\tilde{\sigma}}}_T$ in (60) (notice that this is always possible since $\operatorname{tr} E_4^1(T) = \mathscr{P}_1(T)/\mathbf{R}$), by Cauchy–Schwarz inequality and a scaling argument we get

$$|\mathrm{tr}\,\underline{\underline{\tilde{\sigma}}}_T|_{0,T}^2 = -\int_T \underline{\nabla}(\mathrm{tr}\,\underline{\underline{\tilde{\sigma}}}_T)\cdot\underline{v} \leqslant |\underline{v}|_{0,T}|\underline{\nabla}(\mathrm{tr}\,\underline{\underline{\tilde{\sigma}}}_T)|_{0,T} \leqslant Ch_T^{-1}|\underline{v}|_{0,T}|\mathrm{tr}\,\underline{\underline{\tilde{\sigma}}}_T|_{0,T}. \tag{62}$$

Since $\underline{\underline{\tilde{\sigma}}}_T^D = 0$, it follows $|\mathrm{tr}\,\underline{\underline{\tilde{\sigma}}}_T|_{0,T} = \sqrt{2}|\underline{\underline{\tilde{\sigma}}}_T|_{0,T}$. Therefore, from (62) we obtain

$$|\underline{\underline{\tilde{\sigma}}}_T|_{0,T} \leqslant Ch_T^{-1}|\underline{v}|_{0,T}. \tag{63}$$

If we set

$$\Pi_h\underline{v} = \Pi_2(\underline{v} - \Pi_1\underline{v}) + \Pi_1\underline{v} \quad \forall\underline{v}\in V,$$

from (57), (63) and the features of Clément's operator Π_1, it is easily seen that Π_h verifies (55) and (56). The proof is complete. □

Theorem 4 and Proposition 7 lead to the following result.

Proposition 9. For the method detailed by (47)–(51) and provided that the solution of the continuous problem is sufficiently regular, we have the error estimate

$$\|\underline{u} - \underline{u}_h\|_1 + |p - p_h|_0 \leqslant Ch. \tag{64}$$

Moreover, under assumptions (34) it holds

$$|\underline{u} - \underline{u}_h|_0 \leqslant Ch^2. \tag{65}$$

5. Numerical tests

In this Section we investigate the computational performances of the *mixed-enhanced* elements introduced in Section 4 and based on Formulation (5). We denote our *triangular* schemes with:

- *T*3*E*4(*I*)/*T*3—Element with piecewise linear and continuous approximation for both the displacements and the pressure, enriched by means of the *first set* of Enhanced Strains (cf. (50) and (51)).
- *T*3*E*4(*II*)/*T*3—Element with piecewise linear and continuous approximation for both the displacements and the pressure, enriched by means of the *second set* of Enhanced Strains (cf. (52) and (53)).

For comparison purposes, in the sequel we also consider the following methods.

Non-mixed elements

- *T*3—Standard displacement-based triangular element with piecewise linear and continuous approximation.
- *Q*4—Standard displacement-based quadrilateral element with piecewise bilinear and continuous approximation.
- *Q*4*E*6—Quadrilateral element with piecewise bilinear and continuous approximation for the displacements, enriched by the Enhanced Strains proposed in [13].

Mixed elements

- *T*3/*T*3—Triangular element with piecewise linear and continuous approximation for both the displacements and the pressure.
- *Q*4/*Q*4—Quadrilateral element with piecewise bilinear and continuous approximation for both the displacements and the pressure.

- $Q4E6/Q4$—Quadrilateral element with piecewise bilinear and continuous approximation for both the displacements and the pressure, enriched by means of the Enhanced Strains proposed in [13] (Pantuso–Bathe element).

Moreover, we express forces and lengths in *KN* and *m*, respectively.

5.1. Fully constrained block

We propose a couple of tests in order to numerically assess the convergence rates of the triangular $T3E4(I)/T3$ and $T3E4(II)/T3$ elements, comparing the results with the quadrilateral $Q4E6/Q4$ element.

We consider a fully constrained square block of incompressible material ($\lambda/\mu = +\infty$), occupying the region $\Omega = (-L,L)\times(-L,L)$. Each test consists in choosing a particular body load $\underline{f}$ for which the corresponding analytical solution $(\underline{u},p)$ is available.

Fig. 1 shows the generic adopted mesh for undistorted quadrilaterals, distorted quadrilaterals and triangles, respectively. It is clearly seen that:

- the undistorted quadrilateral mesh simply consists in $n\times n$ equal sub-squares (see Fig. 1(left));
- the distorted quadrilateral mesh is obtained from the undistorted one, essentially by moving the point of coordinates (0,0) to the point of coordinates $(L/2,L/2)$ (see Fig. 1(middle));
- the triangular mesh is obtained from the undistorted quadrilateral mesh, splitting each sub-square into two triangles by means of a diagonal (see Fig. 1(right)).

In all the numerical experiments, we choose $n = 8, 16, 32, 64, 128$; we also point out that n (i.e. the number of subdivisions per direction) behaves as h^{-1}.

Moreover, since the body is fully constrained, the pressure is defined up to a constant, which is fixed in our computations by imposing $\int_\Omega p_h = 0$.

Finally, the results obtained using the $Q4E6/Q4$ element with distorted meshes are here below labelled with "$Q4E6/Q4$ (dist)".

5.1.1. Polynomial load test

For this problem we set:

$$L = 1, \quad \mu = 40$$

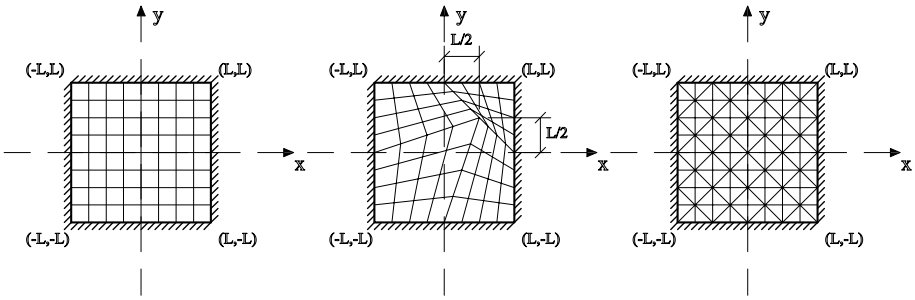

Fig. 1. Fully constrained block. Problem geometry and boundary conditions. Undistorted quadrilateral, distorted quadrilateral and triangular meshes.

$$f_1 = \mu y\left(-\frac{3}{2}x^4 + 6x^2 - 3x^2y^2 + y^2 - \frac{5}{2}\right) - 15x^2(y-1)$$

$$f_2 = \mu x\left(\frac{3}{2}y^4 - 6y^2 + 3y^2x^2 - x^2 + \frac{5}{2}\right) - 3y^2 - 5x^3,$$

where f_1 and f_2 are the components of the body load $\underline{f}$. Accordingly, the analytical solution is:

$$u_1 = \frac{(x^2-1)^2(y^2-1)y}{4}$$

$$u_2 = \frac{(y^2-1)^2(1-x^2)x}{4}$$

$$p = 5x^3(y-1) + y^3.$$

For all the considered schemes, Figs. 2–4 report the computed relative errors versus n, in log–log scale.

More precisely, Figs. 2 and 3 show the L^2-norm convergence rates for $\underline{u}$ and p, respectively. Furthermore, Fig. 4 gives the energy-norm convergence rate for $\underline{u}$. The energy-norm is here defined as

$$\|\underline{u}\|_{en} := \left(2\mu \int_\Omega \underline{\underline{\varepsilon}}(\underline{u}) : \underline{\underline{\varepsilon}}(\underline{u})\right)^{1/2}, \tag{66}$$

which is clearly equivalent to the H^1-norm, due to Korn's inequality.

For all the elements under investigation, we observe that:

- The displacement L^2-norm convergence rate is $O(h^2)$, as predicted by the theory.
- The pressure L^2-norm convergence rate is $O(h^{3/2})$, while the theoretical estimate gives only $O(h)$. However, we conjecture this is a super-convergence effect, probably due to the adopted meshes, and it does not show up in general situations.
- The displacement energy-norm convergence rate is $O(h)$, again as predicted by the theory.

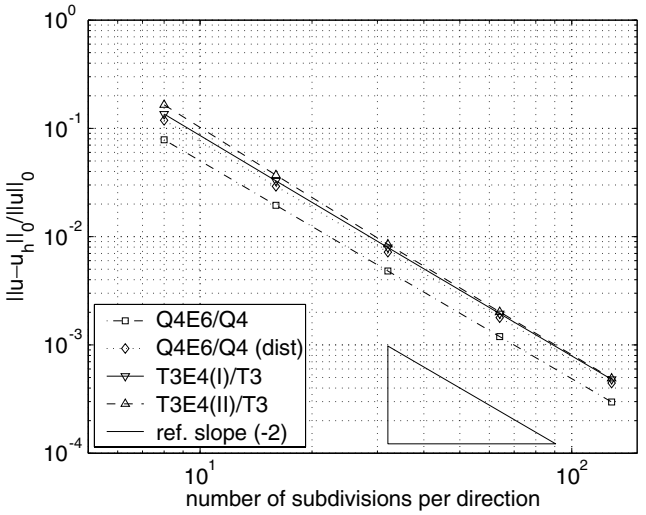

Fig. 2. Fully constrained block. Polynomial load test. L^2-norm convergence rate for $\underline{u}$.

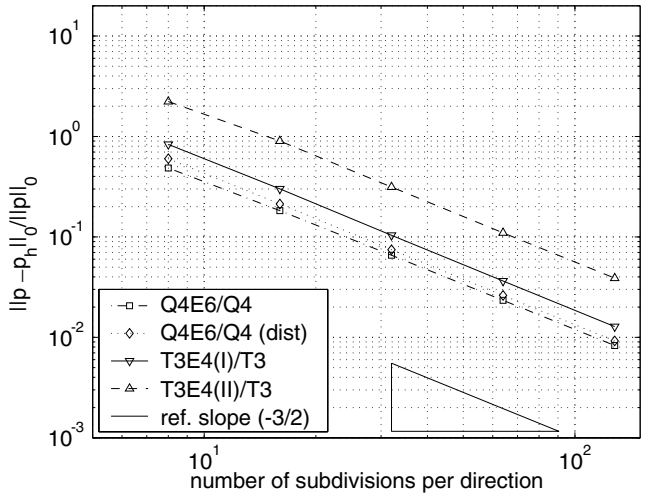

Fig. 3. Fully constrained block. Polynomial load test. L^2-norm convergence rate for p.

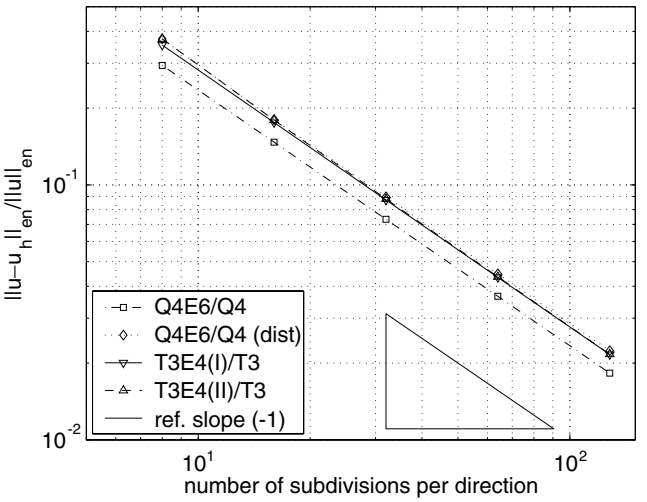

Fig. 4. Fully constrained block. Polynomial load test. Energy-norm convergence rate for $\underline{u}$.

Even if all the schemes share *the same convergence rates*, we point out that the undistorted $Q4E6/Q4$ element delivers the best performances. Moreover, the $T3E4(I)/T3$ element essentially behaves as the distorted $Q4E6/Q4$ (dist) element, while the $T3E4(II)/T3$ element returns higher relative errors for the pressure fields.

5.1.2. Trigonometric load test

For this second problem we set:

$$L = \pi/2, \quad \mu = 40$$

$$f_1 = \mu \cos y \sin y(1 - 4\cos^2 x) - 2xy\cos(x^2 y)$$

$$f_2 = -\mu \cos x \sin x(1 - 4\cos^2 y) - x^2 \cos(x^2 y),$$

such that the analytical solution is:

$$u_1 = -\frac{\cos^2 x \cos y \sin y}{2}$$

$$u_2 = \frac{\cos^2 y \cos x \sin x}{2}$$

$$p = \sin(x^2 y).$$

In Figs. 5–7 we report the corresponding computed relative errors versus n, in log–log scale. We remark that all the considerations concerning the first test apply also to this case.

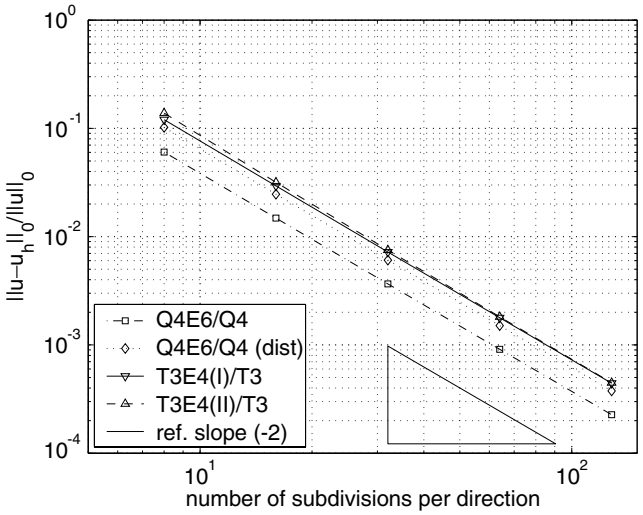

Fig. 5. Fully constrained block. Trigonometric load test. L^2-norm convergence rate for $\underline{u}$.

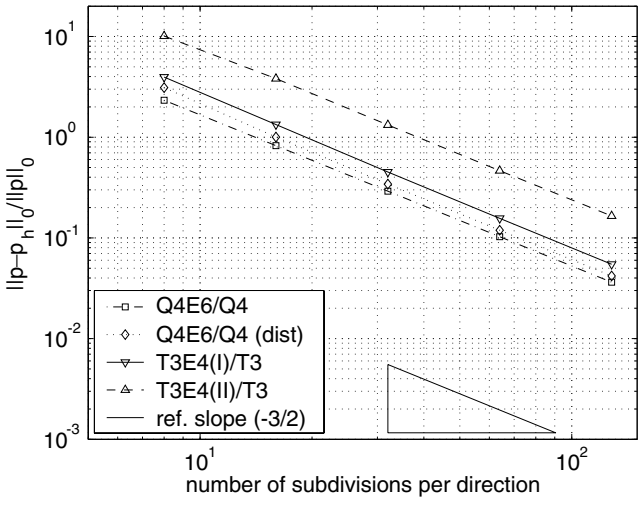

Fig. 6. Fully constrained block. Trigonometric load test. L^2-norm convergence rate for p.

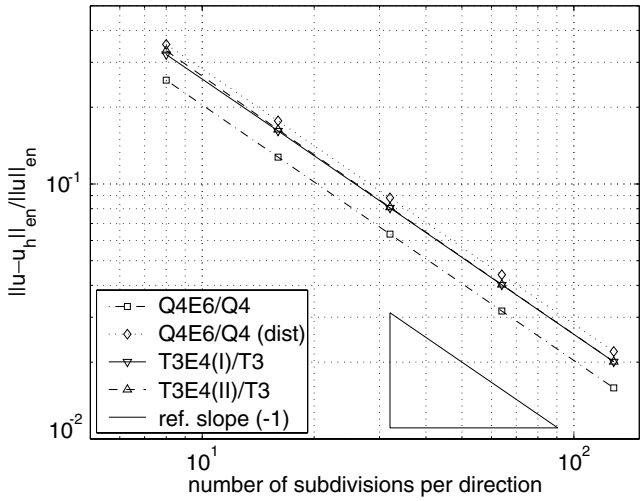

Fig. 7. Fully constrained block. Trigonometric load test. Energy-norm convergence rate for $\underline{\underline{u}}$.

5.2. Bending test

The problem consists in the analysis of a beam of length $L = 10$ and height $H = 2$ under pure bending (Fig. 8). We point out that, as in Ref. [9] (see the Example on pages 248–249), our goal is to assess the *volumetric* locking behaviour of the elements under investigation in bending dominated problems and not their locking properties in *shear* (see Ref. [1] for a detailed discussion of volumetric versus shear locking).

The beam is first divided into two subdomains Ω_1 and Ω_2. According to Fig. 8, we obtain a quadrilateral grid, labelled as "$n \times n$ mesh", by meshing *each subdomain* with $n \times n$ quadrilaterals; a corresponding triangular grid, still labelled as "$n \times n$ mesh" for simplicity, is obtained splitting each quadrilateral element into two triangles by means of a diagonal. Moreover, it is possible to introduce a distortion in the shape of the two subdomains by means of a parameter $a \neq 0$, as shown in Fig. 8. In the following we will consider:

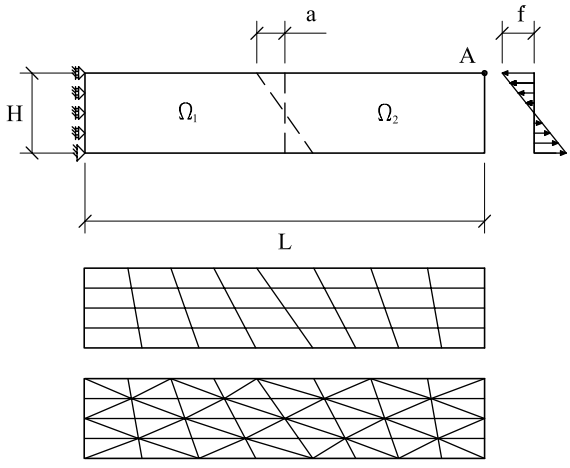

Fig. 8. Bending test. Problem geometry, boundary and loading conditions. Distorted 4×4 meshes.

- the undistorted case (i.e. $a = 0$);
- a distorted case with $a = 0.5$.

We perform the test using the elements presented at the beginning of this Section and we study their behaviours for compressible ($\lambda/\mu = 1$), nearly incompressible ($\lambda/\mu = 10^7$) or incompressible ($\lambda/\mu = +\infty$) materials, reporting the following quantities:

- the full elastic energy E associated with the problem, computed as the inner product between the internal force and the solution vector;
- the displacements $u_1(A)$ and $u_2(A)$ of the specific node indicated by letter A in Fig. 8;
- the pressure $p(A)$ at node A (for mixed formulations).

5.2.1. Compressible case

We consider a compressible material with $\lambda = 40$ and $\mu = 40$, reporting the results of the analyses in Tables 1 and 2.

As the analytical solution is not available, we consider as reference solutions the following values, obtained using the $Q4E6/Q4$ element with the fine 128×128 mesh and $a = 0.5$:

$$E = 5.6250 \times 10^{-3}$$
$$u_1(A) = -2.8125 \times 10^{-1}$$
$$u_2(A) = 1.4062$$
$$p(A) = -7.5000 \times 10^{-1}.$$

According to [20], we notice that the enhanced $Q4E6$ and $Q4E6/Q4$ elements exactly reproduce the reference solutions using a mesh of just two *undistorted* quadrilaterals (1×1 mesh). Instead, this property is not fulfilled by the mixed-enhanced triangular elements.

Table 1
Bending test

Element	Output		1×1		4×4	16×16	64×64
			$a = 0$	$a = 0.5$	$a = 0.5$		
$Q4$	E	[$\times 10^3$]	1.6216	1.2030	4.6722	5.5538	5.6205
	$u_1(A)$	[$\times 10$]	−0.81081	−0.60150	−2.3227	−2.7736	−2.8098
	$u_2(A)$		0.40541	0.30075	1.1667	1.3882	1.4051
$Q4/Q4$	E	[$\times 10^3$]	1.6216	1.2766	4.7325	5.5594	5.6209
	$u_1(A)$	[$\times 10$]	−0.81081	−0.63828	−2.3527	−2.7764	−2.8100
	$u_2(A)$		0.40541	0.31914	1.1817	1.3896	1.4052
	$p(A)$	[$\times 10$]	−3.2432	−2.6462	−6.5581	−7.2862	−7.4454
$Q4E6$	E	[$\times 10^3$]	5.6250	4.5541	5.6235	5.6250	5.6250
	$u_1(A)$	[$\times 10$]	−2.8125	−2.2770	−2.8117	−2.8125	−2.8125
	$u_2(A)$		1.4062	1.1385	1.4059	1.4062	1.4062
$Q4E6/Q4$	E	[$\times 10^3$]	5.6250	4.7738	5.6238	5.6250	5.6250
	$u_1(A)$	[$\times 10$]	−2.8125	−2.3869	−2.8119	−2.8125	−2.8125
	$u_2(A)$		1.4062	1.1934	1.4060	1.4062	1.4062
	$p(A)$	[$\times 10$]	−7.5000	−6.3648	−7.5107	−7.5000	−7.5000

Quadrilateral elements with $\lambda/\mu = 1$. Undistorted ($a = 0$) and distorted ($a = 0.5$) 1×1 meshes, distorted ($a = 0.5$) 4×4, 16×16 and 64×64 meshes.

Table 2
Bending test

Element	Output		1×1		4×4	16×16	64×64
			$a=0$	$a=0.5$	$a=0.5$		
$T3$	E	$[\times10^3]$	0.58387	0.71578	3.6527	5.4399	5.6130
	$u_1(A)$	$[\times10]$	−0.29194	−0.35789	−1.8076	−2.7125	−2.8055
	$u_2(A)$		0.14597	0.17894	0.90983	1.3595	1.4032
$T3/T3$	E	$[\times10^3]$	0.60856	0.71779	3.6899	5.4455	5.6134
	$u_1(A)$	$[\times10]$	−0.30428	−0.35889	−1.8257	−2.7153	−2.8057
	$u_2(A)$		0.15214	0.17945	0.91912	1.3609	1.4033
	$p(A)$	$[\times10]$	−1.1150	−0.21334	−3.7991	−6.5394	−7.2605
$T3E4(I)/T3$	E	$[\times10^3]$	0.61437	0.71833	3.7051	5.4478	5.6134
	$u_1(A)$	$[\times10]$	−0.30718	−0.35916	−1.8331	−2.7164	−2.8057
	$u_2(A)$		0.15359	0.17958	0.92288	1.3614	1.4033
	$p(A)$	$[\times10]$	−0.65391	−0.09082	−3.9324	−6.6128	−7.2780
$T3E4(II)/T3$	E	$[\times10^3]$	0.61213	0.71805	3.6986	5.4469	5.6135
	$u_1(A)$	$[\times10]$	−0.30606	−0.35903	−1.8299	−2.7160	−2.8057
	$u_2(A)$		0.15303	0.17951	0.92127	1.3612	1.4033
	$p(A)$	$[\times10]$	−0.81357	−0.13990	−3.7377	−6.5448	−7.2618

Triangular elements with $\lambda/\mu = 1$. Undistorted ($a = 0$) and distorted ($a = 0.5$) 1×1 meshes, distorted ($a = 0.5$) 4×4, 16×16 and 64×64 meshes.

5.2.2. Nearly incompressible and incompressible cases

We consider nearly incompressible and incompressible materials, choosing $\lambda = 40\times10^7$ and $\lambda = +\infty$, respectively; in addition, we set $\mu = 40$ for both cases. In these situations, only the mixed-enhanced schemes are efficient (among the ones presented in this Section). Therefore, we focus only on the $Q4E6/Q4$, $T3E4(I)/T3$ and $T3E4(II)/T3$ elements, as shown in Tables 3 and 4. Moreover, we point out that the numerical results delivered in the nearly incompressible and incompressible cases are exactly the same.

Table 3
Bending test

Element geometry	Element	Output		1×1	4×4	16×16	64×64
				$a=0$	$a=0.5$		
Quadrilateral	$Q4E6/Q4$	E	$[\times10^3]$	3.7500	3.7495	3.7500	3.7500
		$u_1(A)$	$[\times10]$	−1.8750	−1.8748	−1.8750	−1.8750
		$u_2(A)$	$[\times10]$	9.3750	9.3737	9.3750	9.3750
		$p(A)$		−1.5000	−1.5016	−1.5000	−1.5000
Triangular	$T3E4(I)/T3$	E	$[\times10^3]$	0.60097	2.8583	3.6788	3.7455
		$u_1(A)$	$[\times10]$	−0.30048	−1.4158	−1.8356	−1.8723
		$u_2(A)$	$[\times10]$	1.5024	7.1279	9.1951	9.3634
		$p(A)$		−0.15465	−0.89369	−1.3483	−1.4620
	$T3E4(II)/T3$	E	$[\times10^3]$	0.57811	2.8220	3.6753	3.7453
		$u_1(A)$	$[\times10]$	−0.28905	−1.3979	−1.8338	−1.8721
		$u_2(A)$	$[\times10]$	1.4453	7.0376	9.1863	9.3629
		$p(A)$		−0.32372	−0.72864	−1.2964	−1.4495

Quadrilateral and triangular elements with $\lambda/\mu = 10^7$. Undistorted ($a = 0$) 1×1 mesh and distorted ($a = 0.5$) 4×4, 16×16 and 64×64 meshes.

Table 4
Bending test

Element geometry	Element	Output		1×1	4×4	16×16	64×64
				$a=0$	$a=0.5$		
Quadrilateral	$Q4E6/Q4$	E	[$\times10^3$]	3.7500	3.7495	3.7500	3.7500
		$u_1(A)$	[$\times10$]	−1.8750	−1.8748	−1.8750	−1.8750
		$u_2(A)$	[$\times10$]	9.3750	9.3737	9.3750	9.3750
		$p(A)$		−1.5000	−1.5016	−1.5000	−1.5000
Triangular	$T3E4(I)/T3$	E	[$\times10^3$]	0.60097	2.8583	3.6788	3.7455
		$u_1(A)$	[$\times10$]	−0.30048	−1.4158	−1.8356	−1.8723
		$u_2(A)$	[$\times10$]	1.5024	7.1279	9.1951	9.3634
		$p(A)$		−0.15465	−0.89369	−1.3483	−1.4620
	$T3E4(II)/T3$	E	[$\times10^3$]	0.57811	2.8220	3.6753	3.7453
		$u_1(A)$	[$\times10$]	−0.28905	−1.3979	−1.8338	−1.8721
		$u_2(A)$	[$\times10$]	1.4453	7.0376	9.1863	9.3629
		$p(A)$		−0.32372	−0.72864	−1.2964	−1.4495

Quadrilateral and triangular elements with $\lambda/\mu = +\infty$. Undistorted ($a = 0$) 1×1 mesh and distorted ($a = 0.5$) 4×4, 16×16 and 64×64 meshes.

As before, we consider as reference solutions the following values, obtained using the $Q4E6/Q4$ element with the 128×128 mesh and $a = 0.5$:

$$E = 3.7500\times10^{-3}$$
$$u_1(A) = -1.8750\times10^{-1}$$
$$u_2(A) = 9.3750\times10^{-1}$$
$$p(A) = -1.5000.$$

Also here, we notice that the *undistorted* quadrilateral 1×1 mesh exactly reproduces the reference solutions.

As a final remark, we observe that for this bending test the $Q4E6/Q4$ element gives the best results.

5.3. Cook's membrane

The last problem under investigation is the so-called Cook's membrane (Fig. 9), which is another classical bending dominated test introduced here to assess element performances with respect to volumetric locking. Following Ref. [15], we set $L = 48$, $H_1 = 44$, $H_2 = 16$ and $F = 1$, where F is the resultant of the uniformly distributed shear load f.

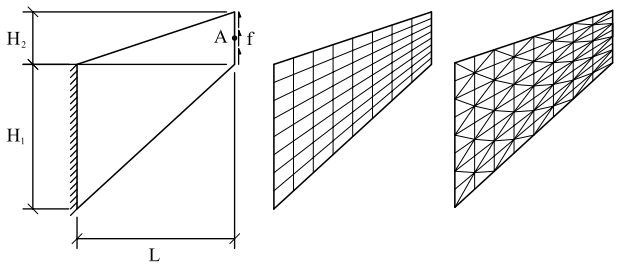

Fig. 9. Cook's membrane. Problem geometry, boundary and loading conditions. 8×8 meshes.

Table 5
Cook's membrane

Element geometry	Element	Output		4×4	16×16	64×64
Quadrilateral	*Q4E6*	E	[×10]	2.0606	2.1465	2.1573
		$u_1(A)$		−9.0798	−9.5273	−9.5718
		$u_2(A)$	[$\times10^{-1}$]	2.0591	2.1424	2.1510
	Q4E6/Q4	E	[×10]	2.0741	2.1487	2.1576
		$u_1(A)$		−9.1495	−9.5387	−9.5737
		$u_2(A)$	[$\times10^{-1}$]	2.0724	2.1444	2.1513
		$p(A)$	[$\times10^{2}$]	3.3763	4.4639	4.7070
Triangular	*T3E4(I)/T3*	E	[×10]	1.5634	2.0911	2.1527
		$u_1(A)$		−6.3466	−9.2612	−9.5513
		$u_2(A)$	[$\times10^{-1}$]	1.5631	2.0901	2.1470
		$p(A)$	[$\times10^{2}$]	1.3276	3.0945	4.2997
	T3E4(II)/T3	E	[×10]	1.5533	2.0895	2.1525
		$u_1(A)$		−6.2907	−9.2544	−9.5506
		$u_2(A)$	[$\times10^{-1}$]	1.5526	2.0887	2.1469
		$p(A)$	[$\times10^{2}$]	0.89457	2.5825	4.0269

Quadrilateral and triangular elements with $\lambda/\mu = 2$. Meshes: 4×4, 16×16 and 64×64.

We perform the test for compressible ($\lambda/\mu = 2$), nearly incompressible ($\lambda/\mu = 2\times10^7$) and incompressible ($\lambda/\mu = +\infty$) materials and we report the same quantities described in the Section 5.2.

5.3.1. Compressible case

We consider a compressible material with $\lambda = 0.75$ and $\mu = 0.375$, reporting the results of the analyses in Table 5.

Similarly to the bending test previously described, the analytical solution is not available. Therefore, we consider as reference solutions the following values, obtained using the *Q4E6/Q4* element with the 128×128 mesh:

$$E = 2.1585\times10^{-1}$$
$$u_1(A) = -9.5775$$
$$u_2(A) = 2.1520\times10^{1}$$
$$p(A) = 4.7192\times10^{-2}.$$

5.3.2. Nearly incompressible and incompressible cases

We consider nearly incompressible and incompressible materials, choosing $\lambda = 0.75\times10^7$ and $\lambda = +\infty$, respectively; moreover, we set $\mu = 0.375$ for both cases. As for the corresponding bending tests in nearly incompressible and incompressible regimes, only the mixed-enhanced elements have been examined, as reported in Tables 6 and 7. Again, the numerical results for the nearly incompressible and the incompressible cases are exactly the same.

Furthermore, the reference solutions obtained using the *Q4E6/Q4* element with the 128×128 mesh are:

$$E = 1.6491\times10^{-1}$$
$$u_1(A) = -7.2480$$
$$u_2(A) = 1.6442\times10^{1}$$
$$p(A) = 7.0788\times10^{-2}.$$

Table 6
Cook's membrane

Element geometry	Element	Output		4×4	16×16	64×64
Quadrilateral	$Q4E6/Q4$	E	[×10]	1.5705	1.6359	1.6476
		$u_1(A)$		−6.7483	−7.1747	−7.2393
		$u_2(A)$	[$\times10^{-1}$]	1.5658	1.6324	1.6428
		$p(A)$	[$\times10^{2}$]	5.3185	6.6875	7.0606
Triangular	$T3E4(I)/T3$	E	[×10]	1.2693	1.5995	1.6435
		$u_1(A)$		−5.0490	−6.9812	−7.2170
		$u_2(A)$	[$\times10^{-1}$]	1.2662	1.5980	1.6391
		$p(A)$	[$\times10^{2}$]	2.4461	4.8216	6.4739
	$T3E4(II)/T3$	E	[×10]	1.2263	1.5917	1.6424
		$u_1(A)$		−4.7921	−6.9412	−7.2105
		$u_2(A)$	[$\times10^{-1}$]	1.2218	1.5909	1.6381
		$p(A)$	[$\times10^{2}$]	0.74186	2.0316	4.6121

Quadrilateral and triangular elements with $\lambda/\mu = 2\times10^{7}$. Meshes: 4×4, 16×16 and 64×64.

Table 7
Cook's membrane

Element geometry	Element	Output		4×4	16×16	64×64
Quadrilateral	$Q4E6/Q4$	E	[×10]	1.5705	1.6359	1.6476
		$u_1(A)$		−6.7483	−7.1747	−7.2393
		$u_2(A)$	[$\times10^{-1}$]	1.5658	1.6324	1.6428
		$p(A)$	[$\times10^{2}$]	5.3185	6.6875	7.0606
Triangular	$T3E4(I)/T3$	E	[×10]	1.2693	1.5995	1.6435
		$u_1(A)$		−5.0490	−6.9812	−7.2170
		$u_2(A)$	[$\times10^{-1}$]	1.2662	1.5980	1.6391
		$p(A)$	[$\times10^{2}$]	2.4461	4.8216	6.4739
	$T3E4(II)/T3$	E	[×10]	1.2263	1.5917	1.6424
		$u_1(A)$		−4.7921	−6.9412	−7.2105
		$u_2(A)$	[$\times10^{-1}$]	1.2218	1.5909	1.6381
		$p(A)$	[$\times10^{2}$]	0.74186	2.0316	4.6121

Quadrilateral and triangular elements with $\lambda/\mu = +\infty$. Meshes: 4×4, 16×16 and 64×64.

The numerical results show that for the Cook's membrane the $Q4E6/Q4$, $T3E4(I)/T3$ and $T3E4(II)/T3$ elements provide robust schemes.

6. Conclusions

We have investigated the Mixed-Enhanced Strain technique within the context of the u/p formulation for linear elasticity problems. We have developed a general theoretical analysis, extending the results presented in [10]; in particular, we have proved optimal uniform error bounds for the L^2-norm of the displacements. We have presented several numerical tests on triangular and quadrilateral elements to assess their computational performances. In particular, the numerical results confirm the convergence rates predicted by the theory.

We conclude recalling that, for quadrilateral elements, the straightforward extension of the Enhanced Strain approach to large deformation problems generally leads to unstable methods (see for example [11,12,14,22]). We conjecture that also triangular elements suffer from the same drawback and possible cures could be obtained by considering the guidelines of [1,17–19], for instance. This will be the subject of future communications.

Acknowledgement

This work has been partially supported by the European Project HPRN-CT-2002-00284 "New Materials, Adaptive Systems and their Nonlinearities. Modelling, Control and Numerical Simulation".

References

[1] F. Armero, On the locking and stability of finite elements in finite deformation plane strain problems, Comput. Struct. 75 (2000) 261–290.
[2] K.J. Bathe, Finite Element Procedures, Prentice Hall, Englewood Cliffs, NJ, 1996.
[3] D. Braess, Enhanced assumed strain elements and locking in membrane problems, Comput. Methods Appl. Mech. Engrg. 165 (1998) 155–174.
[4] D. Braess, C. Carstensen, B.D. Reddy, Uniform convergence and a posteriori estimators for the enhanced strain finite element method, in press.
[5] F. Brezzi, M. Fortin, Mixed and Hybrid Finite Element Methods, Springer-Verlag, New York, 1991.
[6] S.C. Brenner, L.-Y. Sung, Linear finite element methods for planar linear elasticity, Math. Comp. 59 (1992) 321–338.
[7] P.G. Ciarlet, The Finite Element Methods for Elliptic Problems, North-Holland, Amsterdam, 1978.
[8] P. Clément, Approximation by finite element functions using local regularization, RAIRO Anal. Numer. 9 (1975) 77–84.
[9] T.J.R. Hughes, The Finite Element Method, Dover Publications, 2000.
[10] C. Lovadina, Analysis of strain-pressure finite element methods for the Stokes problem, Numer. Methods PDE's 13 (1997) 717–730.
[11] C. Lovadina, F. Auricchio, On the enhanced strain technique for elasticity problems, Comput. Struct. 18 (2003) 777–787.
[12] J.C. Nagtegaal, D.D. Fox, Using assumed enhanced strain elements for large compressive deformation, Int. J. Solids Struct. 33 (1996) 3151–3159.
[13] D. Pantuso, K.J. Bathe, A four-node quadrilateral mixed-interpolated element for solids and fluids, Math. Models Meth. Appl. Sci. 5 (1995) 1113–1128.
[14] D. Pantuso, K.J. Bathe, On the stability of mixed finite elements in large strain analysis of incompressible solids, Finite Elem. Anal. Des. 28 (1997) 83–104.
[15] R. Piltner, R.L. Taylor, Triangular finite elements with rotational degrees of freedom and enhanced strain modes, Comput. Struct. 75 (2000) 361–368.
[16] B.D. Reddy, J.C. Simo, Stability and convergence of a class of enhanced strain methods, SIAM J. Numer. Anal. 32 (6) (1995) 1705–1728.
[17] S. Reese, M. Küssner, B.D. Reddy, A new stabilization technique for finite elements in non-linear elasticity, Int. J. Numer. Meth. Engrg. 44 (1999) 1617–1652.
[18] S. Reese, P. Wriggers, A stabilization technique to avoid hourglassing in finite elasticity, Int. J. Numer. Meth. Engrg. 48 (2000) 79–109.
[19] J.C. Simo, F. Armero, Geometrically nonlinear enhanced strain mixed methods and the method of incompatible modes, Int. J. Numer. Meth. Engrg. 33 (1992) 1413–1449.
[20] J.C. Simo, M.S. Rifai, A class of mixed assumed strain methods and the method of incompatible modes, Int. J. Numer. Meth. Engrg. 29 (1990) 1595–1638.
[21] M. Vogelius, An analysis of the *p*-version of the finite element method for nearly incompressible materials. Uniformly valid, optimal error estimates, Numer. Math. 41 (1983) 39–53.
[22] P. Wriggers, S. Reese, A note on enhanced strain methods for large deformations, Comput. Methods Appl. Mech. Engrg. 135 (1996) 201–209.